The Astrophysical Journal, 715:162–171, 2010 May 20
doi:10.1088/0004-637X/715/1/162

OBSERVED SCALING RELATIONS FOR STRONG LENSING CLUSTERS: CONSEQUENCES FOR COSMOLOGY AND CLUSTER ASSEMBLY

Julia M. Comerford[1], Leonidas A. Moustakas[2], and Priyamvada Natarajan[3,4]
[1] Astronomy Department, 601 Campbell Hall, University of California, Berkeley, CA 94720, USA
[2] Jet Propulsion Laboratory, California Institute of Technology, MS 169-327, 4800 Oak Grove Drive, Pasadena, CA 91109, USA
[3] Department of Astronomy, Yale University, P.O. Box 208101, New Haven, CT 06511, USA
[4] Radcliffe Institute for Advanced Study, Byerly Hall, 8 Garden Street, Cambridge, MA 02138, USA
Received 2009 August 26; accepted 2010 April 2; published 2010 April 26

ABSTRACT

Scaling relations of observed galaxy cluster properties are useful tools for constraining cosmological parameters as well as cluster formation histories. One of the key cosmological parameters, σ_8, is constrained using observed clusters of galaxies, although current estimates of σ_8 from the scaling relations of dynamically relaxed galaxy clusters are limited by the large scatter in the observed cluster mass–temperature (M–T) relation. With a sample of eight strong lensing clusters at $0.3 < z < 0.8$, we find that the observed cluster concentration–mass relation can be used to reduce the M–T scatter by a factor of 6. Typically only relaxed clusters are used to estimate σ_8, but combining the cluster concentration–mass relation with the M–T relation enables the inclusion of unrelaxed clusters as well. Thus, the resultant gains in the accuracy of σ_8 measurements from clusters are twofold: the errors on σ_8 are reduced and the cluster sample size is increased. Therefore, the statistics on σ_8 determination from clusters are greatly improved by the inclusion of unrelaxed clusters. Exploring cluster scaling relations further, we find that the correlation between brightest cluster galaxy (BCG) luminosity and cluster mass offers insight into the assembly histories of clusters. We find preliminary evidence for a steeper BCG luminosity–cluster mass relation for strong lensing clusters than the general cluster population, hinting that strong lensing clusters may have had more active merging histories.

Key words: cosmological parameters – dark matter – galaxies: clusters: individual (3C 220, A 370, Cl 0024, Cl 0939, Cl 2244, MS 0451, MS 1137, MS 2137) – galaxies: evolution – galaxies: formation – gravitational lensing: strong

Online-only material: color figure

1. INTRODUCTION

As the most massive bound systems known, galaxy clusters provide an important link in understanding the composition and growth of structure in the universe. Clusters follow a variety of observational scalings of mass with temperature, luminosity, or cluster counts, and these scalings are sensitive to cosmological parameters including the matter density parameter Ω_{m}, the cosmological constant density parameter Ω_Λ, the dark energy equation-of-state parameter w, and the normalization of the matter power spectrum σ_8 (e.g., Haiman et al. 2001; Bahcall & Comerford 2002; Levine et al. 2002; Schuecker et al. 2003; Allen et al. 2004; Vikhlinin et al. 2009). Such constraints from galaxy clusters complement the constraints on cosmological parameters from Type Ia supernovae and cosmic microwave background observations.

However, useful galaxy cluster constraints on cosmological parameters depend primarily on accurate determinations of cluster masses. Observationally, cluster masses are typically measured in one of three ways.

A long-established method for determining cluster masses employs the virial theorem and the measurement of velocities of the galaxies that constitute the cluster. Based on the three assumptions that the cluster is in virial equilibrium, the galaxy distribution efficiently traces the cluster mass distribution, and the velocity dispersions σ of the galaxies are isotropic, the cluster mass contained within a radius r is estimated $M \sim \sigma^2 r/G$. However, these mass estimates may be biased as a result of galaxy velocity anisotropies or if the galaxy distribution does not follow the total mass distribution (e.g., Bailey 1982).

A second method uses cluster X-ray emission as a tracer of cluster masses. The hot intracluster gas, which is the dominant baryonic component of a cluster and is typically twice the mass of the total mass of the galaxies in a cluster, emits X-rays via bremsstrahlung radiation and atomic line emission. With the temperature T and radial density $\rho(r)$ profiles determined from X-ray spectra and surface brightness distributions, the cluster mass is given by $M \sim r^2/\rho(r)\ d(-\rho T)/dr$. This method assumes that the intracluster gas is spherically distributed and is in hydrostatic equilibrium (Evrard et al. 1996). However, these assumptions may be incorrect. If the gas distribution is not spherical, X-ray mass estimates will be biased by projection effects. Many galaxy clusters are also not in hydrostatic equilibrium, in particular dynamically unrelaxed clusters that are undergoing mergers. There is evidence that the bias of hydrostatic equilibrium mass is linked to the dynamical state of the galaxy cluster (e.g., Andersson et al. 2009; Zhang et al. 2009). In addition, the hot gas of galaxy clusters with buoyant bubbles near their cores might indicate a departure from hydrostatic equilibrium (e.g., Churazov et al. 2001).

The most direct estimates of cluster masses employ gravitational lensing distortions of background galaxies. This technique is free of assumptions about the dynamical state of the cluster, which enables it in principle to yield more consistent mass estimates, though it is also sensitive to projection effects. More accurate cluster mass estimates can in turn provide tighter constraints on cosmological parameters, and therefore it is of key importance to reduce the errors in cluster mass estimates.

For example, the primary source of error in cluster-based determinations of σ_8 is the error in the mass–temperature relation for relaxed clusters (e.g., Pierpaoli et al. 2003; Henry 2004; Voit 2005). Recent studies show that an X-ray-independent mass approach such as gravitational lensing provides a unique tool to calibrate the mass–temperature relation (e.g., Smith et al. 2005; Mahdavi et al. 2008; Zhang et al. 2008). Here, we use strong gravitational lensing mass measurements of a sample of eight strong lensing clusters at $0.3 < z < 0.8$ to accurately measure the galaxy cluster mass–temperature relation. We also include the effects of cluster concentrations in an effort to further reduce the scatter in the cluster mass–temperature relation, which would ultimately enable tighter constraints on σ_8.

In addition to the correlations that exist between cluster properties, some observational properties of brightest cluster galaxies (BCGs) also scale with properties of the host clusters. Whereas scalings between cluster properties are sensitive to cosmological parameters, scalings between BCGs and their host clusters provide constraints on BCG formation and the evolution of clusters.

BCGs are a unique population: they are the most massive and luminous galaxies in the universe. They are typically located near the centers of clusters, which suggests that a BCG's formation history is intricately linked to the formation of the cluster itself. However, the formation of BCGs is still poorly understood.

BCGs may form after their host clusters assemble in one of two ways. First, a BCG may be the first galaxy to be dragged in by dynamical friction to the center of the dark matter halo destined to become a cluster, where it then grows through galactic cannibalism by merging with subsequent galaxies that fall to the center (e.g., Ostriker & Tremaine 1975; Hausman & Ostriker 1978). However, this scenario typically requires more than a Hubble time to form a BCG because much of the mass of the infalling galaxy is tidally stripped, which reduces the dynamical friction effect and slows the infall (Merritt 1985).

BCG formation may also occur after cluster formation if the host cluster's central cooling flow forms stars at the cluster center and those stars build the BCG (Cowie & Binney 1977). There are several instances of ongoing or recent star formation in BCGs that occupy cooling-flow clusters (e.g., Cardiel et al. 1998; Crawford et al. 1999; Hicks & Mushotzky 2005; McNamara et al. 2006), but it is unclear whether the star formation is fueled by the cooling flows or by cold gas brought in through recent galaxy mergers (Bildfell et al. 2008).

In another scenario, BCGs might form in concert with their host clusters. A BCG may begin with several galaxies merging together in a group to form a large galaxy, and then when groups merge as hierarchical structure formation continues, this large galaxy eventually becomes a BCG in a massive cluster (e.g., Merritt 1985; Dubinski 1998; Boylan-Kolchin et al. 2006).

Here, we examine the correlation between BCG luminosity and cluster mass in eight strong lensing clusters at $0.3 < z < 0.8$. This will enable constraints not only on BCG and cluster formation in general, but also on how the BCGs in strong lensing clusters may have formed and evolved differently than BCGs in the general cluster population.

The rest of this paper is organized as follows. In Section 2 we describe the selection of our cluster sample, and Section 3 gives the masses, dynamical states, and X-ray temperatures for these clusters. In Section 4, we find the *M–T* relation for the relaxed clusters in our sample and show how the inclusion of cluster concentrations both significantly reduces the scatter in the *M–T* relation and lifts the restriction on cluster dynamical state. In Section 5, we identify the BCGs in our sample and measure their luminosities. We use these luminosities in Section 6 to measure the correlation between BCG luminosity and cluster mass, and we find preliminary evidence that strong lensing clusters may have more active merging histories than the general cluster population. Section 7 presents our conclusions. Throughout this paper, we adopt a spatially flat cosmological model dominated by cold dark matter and a cosmological constant ($\Omega_m = 0.3$, $\Omega_\Lambda = 0.7$, $h = 0.7$).

2. SAMPLE SELECTION

We base our sample on 10 well-known strong lensing clusters analyzed in Comerford et al. (2006). All 10 clusters have *Hubble Space Telescope* (*HST*) imaging, which make possible the mass determinations and photometry measurements central to this paper. However, there are no published arc redshifts for two of the clusters, Cl 0016+1609 and Cl 0054−27, which limits the strong lensing determination of their cluster masses to the unknown factor D_s/D_{ls}, the ratio of the angular diameter distances to the source and between the lens and source. Consequently, we remove these two clusters, and our sample consists of the remaining eight clusters at $0.3 < z < 0.8$: ClG 2244−02, Abell 370, 3C 220.1, MS 2137.3−2353, MS 0451.6−0305, MS 1137.5+6625, Cl 0939+4713, and ZwCl 0024+1652.

3. CLUSTER PROPERTIES

Strong correlations are found between cluster observables, and the resultant scaling relations clearly encapsulate key information about cosmological parameters and the assembly history of clusters. Cluster masses are a component of many cluster scaling relations, and we measure strong lensing masses for our sample of clusters and compare these to mass estimates from the distributions of cluster X-ray gas. Based on these comparisons and other observable properties of the cluster, we determine the dynamical state of each cluster as relaxed or unrelaxed. We also present cluster X-ray temperatures, which are another component of cluster scaling relations.

3.1. Cluster Strong Lensing Mass Determination

We model each cluster mass distribution with an elliptical Navarro–Frenk–White (NFW; Navarro et al. 1996, 1997) dark matter halo centered on the BCG, using the best-fit NFW parameters found by Comerford et al. (2006). Strong lensing arcs with measured redshifts observed in a cluster constrain its mass distribution, and Comerford et al. (2006) use the arcs to characterize best-fit NFW ellipsoids to each cluster. With the NFW dark matter halos completely defined in this way, we can determine any cluster radius r_Δ as the radius at which the density of the halo is Δ times the critical density at the cluster redshift.

Lack of information about the clusters' three-dimensional shapes prevents us from calculating their elliptical masses, but instead we determine the equivalent mass of a spherical NFW halo. With the Comerford et al. (2006) best-fit scale convergence κ_s and scale radius r_s, we estimate the cluster mass within radius r_Δ as

$$M_\Delta = 4\pi \Sigma_{\rm crit} \kappa_s r_s^2 \left[\ln(1+x) - \frac{x}{1+x} \right] , \tag{1}$$

where $x \equiv r_\Delta / r_s$ and $\Sigma_{\rm crit}$ is the critical surface mass density, defined as

$$\Sigma_{\rm crit} \equiv \frac{c^2}{4\pi G} \frac{D_s}{D_l D_{ls}} , \tag{2}$$

Table 1
Comparisons Between Strong Lensing and X-ray Cluster Mass Estimates

Cluster	Δ	r (h_{70}^{-1} Mpc)	$M_{\rm lens}(\leqslant r)$ ($10^{14}\,h_{70}^{-1}\,M_\odot$)	$M_{\rm X\text{-}ray}(\leqslant r)$ ($10^{14}\,h_{70}^{-1}\,M_\odot$)	$M_{\rm lens}(\leqslant r)/M_{\rm X\text{-}ray}(\leqslant r)$	Reduced χ^2	Dynamical State	Reference
ClG 2244−02	$500\,\Omega^{0.427}$	$0.83^{+0.26}_{-0.20}$	$2.85^{+1.25}_{-0.99}$	$1.50^{+1.07}_{-0.63}$	$1.90^{+2.81}_{-1.18}$	0.91	Relaxed	1
	$18\pi^2\,\Omega^{0.427}$	$1.31^{+0.42}_{-0.31}$	$4.22^{+1.63}_{-1.27}$	$2.37^{+1.73}_{-0.99}$	$1.78^{+2.46}_{-1.06}$	0.86		1
Abell 370	$500\,\Omega^{0.427}$	$1.15^{+0.28}_{-0.20}$	$6.45^{+2.04}_{-1.52}$	$4.19^{+2.06}_{-1.30}$	$1.54^{+1.40}_{-0.75}$	0.85	Unrelaxed	1
	$18\pi^2\,\Omega^{0.427}$	$1.81^{+0.44}_{-0.32}$	$9.25^{+2.50}_{-1.92}$	$6.73^{+3.57}_{-2.16}$	$1.37^{+1.20}_{-0.66}$	0.49		1
3C 220.1	$500\,\Omega^{0.427}$	$1.17^{+0.45}_{-0.25}$	$3.22^{+1.37}_{-0.80}$	$5.80^{+5.25}_{-2.19}$	$0.56^{+0.72}_{-0.34}$	0.44	Relaxed	1
	$18\pi^2\,\Omega^{0.427}$	$1.74^{+0.67}_{-0.37}$	$4.25^{+1.56}_{-0.92}$	$8.64^{+7.85}_{-3.27}$	$0.49^{+0.59}_{-0.29}$	0.59		1
MS 2137.3−2353	2500	$0.46^{+0.02}_{-0.03}$	$1.62^{+0.18}_{-0.19}$	$1.89^{+0.25}_{-0.31}$	$0.86^{+0.28}_{-0.19}$	0.65	Relaxed	2
	$500\,\Omega^{0.427}$	$1.07^{+0.10}_{-0.06}$	$2.73^{+0.34}_{-0.30}$	$3.16^{+0.60}_{-0.36}$	$0.86^{+0.23}_{-0.22}$	0.57		1
	$18\pi^2\,\Omega^{0.427}$	$1.69^{+0.15}_{-0.10}$	$3.40^{+0.40}_{-0.37}$	$4.99^{+0.95}_{-0.57}$	$0.68^{+0.18}_{-0.17}$	3.5		1
MS 0451.6−0305	$500\,\Omega^{0.427}$	$1.38^{+0.25}_{-0.20}$	$13.4^{+3.1}_{-2.6}$	$8.90^{+3.44}_{-2.31}$	$1.50^{+1.00}_{-0.63}$	1.2	Unrelaxed	1
	$18\pi^2\,\Omega^{0.427}$	$2.09^{+0.38}_{-0.30}$	$18.3^{+3.7}_{-3.2}$	$13.6^{+5.4}_{-3.6}$	$1.34^{+0.86}_{-0.55}$	0.68		1
MS 1137.5+6625	$500\,\Omega^{0.427}$	$1.41^{+1.26}_{-0.45}$	$6.80^{+7.22}_{-2.64}$	$12.5^{+32.0}_{-6.7}$	$0.54^{+1.87}_{-0.45}$	0.082	Relaxed	1
	$18\pi^2\,\Omega^{0.427}$	$2.06^{+1.84}_{-0.66}$	$9.10^{+8.34}_{-3.08}$	$18.2^{+46.9}_{-9.8}$	$0.50^{+1.58}_{-0.41}$	0.099		1
Cl 0939+4713		0.36	0.38 ± 0.05	0.72 ± 0.21	$0.53^{+0.31}_{-0.17}$	2.5	Unrelaxed	3
		0.71	0.69 ± 0.08	2.13 ± 0.50	$0.32^{+0.15}_{-0.09}$	8.1		3
ZwCl 0024+1652	$500\,\Omega^{0.427}$	$0.94^{+0.39}_{-0.21}$	$2.02^{+0.97}_{-0.54}$	$2.31^{+2.34}_{-0.91}$	$0.87^{+1.26}_{-0.56}$	0.027	Unrelaxed	1
	$18\pi^2\,\Omega^{0.427}$	$1.45^{+0.61}_{-0.32}$	$2.77^{+1.15}_{-0.64}$	$3.59^{+3.63}_{-1.41}$	$0.77^{+1.03}_{-0.48}$	0.094		1

References. (1) Ota & Mitsuda 2004; (2) Allen et al. 2001; (3) De Filippis et al. 2003.

Table 2
Cluster Lensing Masses and X-ray Temperatures

Cluster	z	M_{200} ($10^{14}\,h_{70}^{-1}\,M_\odot$)	M_{2500} ($10^{14}\,h_{70}^{-1}\,M_\odot$)	kT (keV)	Reference
ClG 2244−02	0.33	4.5 ± 0.9	1.3 ± 0.2	$4.85^{+1.25}_{-0.96}$	1
Abell 370	0.375	9.0 ± 1.0	2.9 ± 0.3	$7.20^{+0.75}_{-0.77}$	1
3C 220.1	0.62	3.1 ± 0.3	0.91 ± 0.10	$5.6^{+1.5}_{-1.1}$	2
MS 2137.3−2353	0.313	2.9 ± 0.4	1.5 ± 0.2	$4.57^{+0.41}_{-0.35}$	1
MS 0451.6−0305	0.55	18 ± 2	6.3 ± 0.7	$8.62^{+1.54}_{-1.21}$	1
MS 1137.5+6625	0.783	6.5 ± 0.7	1.5 ± 0.2	$6.70^{+1.84}_{-1.46}$	1
Cl 0939+4713	0.41	0.71 ± 0.11	0.21 ± 0.03	$7.6^{+2.8}_{-1.6}$	3
ZwCl 0024+1652	0.395	2.3 ± 0.2	0.69 ± 0.07	$5.17^{+1.95}_{-1.34}$	1

References. (1) Horner 2001; (2) Ota et al. 2000; (3) Schindler et al. 1998.

which depends on the angular diameter distances $D_{\rm l}$, $D_{\rm s}$, and $D_{\rm ls}$ from the observer to the lens, to the source, and from the lens to the source, respectively.

We estimate the errors in mass by propagating the errors in the best-fit NFW parameters. As detailed in Comerford et al. (2006) these errors are quite small but are realistic, because the reproduced lensed image is sensitive to slight variations in a parameter's value. However, we note that these errors are relevant only to the choice of lens model and data and do not represent a global systematic uncertainty.

We use the method described here to measure the lensing cluster masses in Table 1, as well as the cluster masses M_{200} and M_{2500} in Table 2.

3.2. Dynamical State of Clusters: Relaxed versus Unrelaxed

Since one of our aims is to measure the mass–temperature relation for relaxed lensing clusters, we must determine which of the eight clusters in our sample are dynamically relaxed. X-ray cluster mass estimates are based on the assumption that the cluster is in hydrostatic equilibrium, and if a cluster is relaxed it is also in hydrostatic equilibrium. Therefore, X-ray mass measurements for relaxed clusters should be accurate and consistent with lensing mass measurements.

We use X-ray mass estimates from the literature, where the X-ray masses are measured for each cluster at two or three different radii. For each cluster, Table 1 gives the lensing mass and X-ray mass measured within the two or three different cluster radii. Table 1 also shows the lensing mass to X-ray mass ratio and the reduced χ^2 of the comparison of lensing and X-ray masses. For six clusters, at all radii at which masses were measured, the ratio of lensing mass to X-ray mass is consistent with unity and the reduced χ^2 is $\lesssim 1$, suggesting that these six clusters could be relaxed. Additional observational evidence in Sections 3.2.1 and 3.2.2 shows that four of these six clusters are relaxed, while the remaining two clusters are unrelaxed.

For at least one of the radii considered, the two clusters MS 2137−23 and Cl 0939+4713 each exhibit lensing to X-ray mass ratios that are inconsistent with unity and reduced χ^2 that are greater than unity, which is evidence that the clusters are unrelaxed. We measure masses for MS 2137−23 within three different radii, and within one of these radii the mass ratio is inconsistent with unity and the reduced χ^2 is greater than unity. However, there is opposing evidence, given in Section 3.2.1, that characterizes MS 2137−23 as a relaxed cluster. For Cl 0939+4713, the mass ratios measured at both radii considered are inconsistent with unity and both reduced χ^2 are much greater than unity, suggesting Cl 0939+4713 may be an unrelaxed cluster. In Section 3.2.2, we present more evidence in support of this conclusion.

Additional information about the dynamical state of a cluster can be found in its X-ray emission map. For example, the position of the BCG relative to the peak in the cluster's X-ray profile may be evidence of a cluster's dynamical state: if the two are coincident the cluster is likely relaxed, otherwise it is likely unrelaxed. The centroid shift is one means of quantifying this positional difference (e.g., Mohr et al. 1993; Jeltema et al. 2008). Additionally, a smooth distribution of X-ray gas indicates the cluster is likely in a relaxed state. However, if the X-ray gas is distributed irregularly or shows evidence of shocks or substructure, the cluster is likely unrelaxed and undergoing a merger. Below we examine evidence for the dynamical state of each cluster individually and label each cluster as relaxed or unrelaxed (these labels are also given in Table 1). We first discuss the four relaxed clusters, then the four unrelaxed clusters.

3.2.1. Relaxed Clusters

1. *Cl 2244−02*. We find that X-ray and lensing masses for Cl 2244−02 are consistent (Table 1) and Ota et al. (1998) also find consistent X-ray and lensing masses, suggesting that hydrostatic equilibrium is a valid assumption for Cl 2244−02 and that it is a relaxed cluster.
2. *3C 220.1*. The radial profile of X-ray emission from 3C 220.1 shows no sign of irregularity and the profile is well fit by a model assuming hydrostatic equilibrium, which suggest that 3C 220.1 is a relaxed cluster (Worrall et al. 2001).
3. *MS 2137−23*. The X-ray and strong lensing masses of MS 2137−23 are in good agreement (Allen 1998), indicating that it is in a relaxed state. Many relaxed clusters also have cooling flows, such as the massive cooling flow in MS 2137−23 (Allen 1998; Wu 2000).
4. *MS 1137+66*. The cluster MS 1137+66 not only has consistent X-ray and weak lensing masses (Table 1), but also has a small centroid shift (Maughan et al. 2008) and may host a moderate cooling flow (Donahue et al. 1999). In addition, Sunyaev Zel'dovich observations of the cluster show no obvious substructure (Cotter et al. 2002). These properties connote that MS 1137+66 is a relaxed cluster.

3.2.2. Unrelaxed Clusters

1. *Abell 370*. Abell 370 hosts two cD galaxies, and there are X-ray peaks centered on each cD (Mellier et al. 1994). The two cD galaxies are moving relative to each other at 1000 km s^{-1}, signaling that Abell 370 is an unrelaxed cluster undergoing a merger (Kneib et al. 1993).
2. *Cl 0939+4713*. X-ray observations of Cl 0939+4713 show evidence for substructure (Schindler & Wambsganss 1996), and the disagreement between lensing and X-ray masses shown in Table 1 further suggests that Cl 0939+4713 is not in hydrostatic equilibrium. These observations indicate Cl 0939+4713 is an unrelaxed cluster.
3. *Cl 0024+17*. The two dark matter clumps near the center of Cl 0024+17 are separated in redshift, implying that it is a merging cluster (Natarajan et al. 2009). There is additional evidence for substructure in Cl 0024+17 in its mass models, which require substructure to produce a good fit to the cluster's lensing arcs (Broadhurst et al. 2000). The redshifts of the member galaxies are distributed bimodally, fortifying the evidence that Cl 0024+17 may have undergone a merger with another cluster (Czoske et al. 2002). The evidence implies that Cl 0024+17 is an unrelaxed cluster.
4. *MS 0451.6−0305*. The distribution of mass within the central 1′ of MS 0451.6−0305 is not smooth, and the centroid shift indicates the BCG is not located at the X-ray peak (Borys et al. 2004; Maughan et al. 2008). These observations suggest that MS 0451.6−0305 is unrelaxed.

3.3. Cluster X-ray Temperatures

The temperature of the intracluster medium is commonly measured using its X-ray emission in one of several ways: through fits to the cluster's observed X-ray spectrum (yielding the spectroscopic temperature T_s), through weighting by the mass of the gas element (yielding the mass-weighted temperature T_m), or through weighting by the emissivity of the gas element (yielding the emission-weighted temperature T_{em}). However, the spectroscopic temperature T_s is systematically lower than the mass-weighted temperature T_m and the emission-weighted temperature T_{em} (Mathiesen & Evrard 2001; Mazzotta et al. 2004), so an accurate temperature comparison across different clusters requires consistent temperature measurements.

To ensure that the cluster temperatures we use for our sample are as consistent as possible, we use the mean cluster temperatures derived from the single-temperature model fits of *ASCA* data in Horner (2001). This large, homogeneous catalog of spectroscopic cluster temperatures includes six of our clusters, and for the remaining two clusters, 3C 220.1 and Cl 0939+4713, we remain as consistent as possible by using spectroscopic temperatures from single-temperature fits. Table 2 gives the cluster temperatures and the corresponding references. We note that none of the temperatures we use apply corrections for cool cores at the cluster centers.

Some clusters in our sample also have temperature measurements from *Chandra* and *XMM-Newton* data. Specifically, 3C 220.1 has a *Chandra* temperature of $8.5^{+3.7}_{-2.3}$ keV within 10″–45″ (Worrall et al. 2001); MS 0451.6−0305 has a *Chandra* temperature of $6.7^{+0.6}_{-0.5}$ keV within r_{500} (Maughan et al. 2008); MS 1137.5+6625 has a *Chandra* temperature of $5.8^{+0.7}_{-0.6}$ keV within r_{500} (Maughan et al. 2008); and Cl 0024+17 has an average *Chandra* temperature of $4.47^{+0.83}_{-0.54}$ keV (Ota et al. 2004) and an *XMM-Newton* temperature of 3.52 ± 0.17 keV within 3′ (Zhang et al. 2005). Use of *Chandra* or *XMM-Newton* temperatures could change the results of the mass–temperature relation. However, because *Chandra* and *XMM-Newton* temperatures have been measured for only a subset of our sample, and because these temperatures are measured within inconsistent cluster radii, we do not use *Chandra* and *XMM-Newton* measurements in our determination of the cluster mass–temperature relation below.

4. THE MASS–TEMPERATURE RELATION

Theoretical arguments suggest a correlation between cluster mass and X-ray temperature for relaxed clusters, which provides the link between the gas in a cluster and its mass. Here we determine the cluster mass–temperature relation for relaxed *strong lensing* clusters, and we also explore the correlation

Table 3
Power-law Fits to the M–T Relation

A	α	Method[a]	kT (keV)[b]	Sample	Reference
1.60 ± 3.42	1.43 ± 1.28	SL	$4.6 < T_s < 6.7$	Four relaxed SL clusters	1
2.0 ± 0.29	$1.34^{+0.30}_{-0.28}$	WL	$3.6 < T_s < 9.8$	17 WL clusters	2
1.79 ± 0.07	1.64 ± 0.06	X-ray	$0.7 < T_s < 8.9$	13 relaxed clusters	3
2.06 ± 0.10	1.58 ± 0.07	X-ray	$0.6 < T_m < 9.3$	13 relaxed clusters	3
1.69 ± 0.05	1.70 ± 0.07	X-ray	$2.2 < T_s < 8.3$	10 relaxed clusters	4
1.79 ± 0.06	1.51 ± 0.11	X-ray	$3.7 < T_s < 8.3$	Six relaxed clusters	4
1.88 ± 0.26	1.52 ± 0.36	X-ray	$5.6 < T_m < 15.3$	Five relaxed WL or SL clusters	5
1.97 ± 0.07	1.54 ± 0.02	Simulation	T_m	$M_{2500} > 4 \times 10^{14}\, h_{70}^{-1}\, M_\odot$ clusters in hydrodynamics simulation	6

Note.
[a] Method used to determine the cluster mass, where SL is strong lensing and WL is weak lensing.
[b] Temperature range of the cluster sample, where T_s is the spectroscopic temperature and T_m is the mass-weighted temperature.
References. (1) This paper; (2) Hoekstra 2007; (3) Vikhlinin et al. 2006; (4) Arnaud et al. 2005; (5) Allen et al. 2001; (6) Kay et al. 2005.

between the scatter in cluster temperature and the scatter in cluster concentration to establish a general mass–temperature relation that is independent of the dynamical state of the clusters.

4.1. The M–T Relation for Relaxed Strong Lensing Clusters

A correlation between cluster mass and cluster X-ray gas temperature in relaxed clusters is expected as a direct consequence of theoretical arguments. If a cluster's X-ray gas is in virial and hydrostatic equilibrium, then the theoretical expectation is that cluster mass scales with X-ray temperature as $E(z)M_\Delta = A(\Delta)T^{1.5}$, where $E(z) = H(z)/H_0 = \sqrt{\Omega_m(1+z)^3 + \Omega_\Lambda}$ for a flat universe, M_Δ is the cluster mass within the radius where the mean mass density is Δ times the critical density, and $A(\Delta)$ is the Δ-dependent normalization.

The critical overdensity $\Delta = 2500$ is commonly used in cluster analyses because in the central regions enclosed by r_{2500}, *Chandra* cluster temperature profiles can be measured even at high redshifts (e.g., up to $z = 0.9$ in Allen et al. 2004). The overdensity $\Delta = 2500$ is therefore appropriate for our cluster sample, which extends to $z = 0.8$. Using the overdensity $\Delta = 2500$, we can write the cluster mass–temperature relation in power-law form as

$$E(z)\left(\frac{M_{2500}}{10^{14}\, h_{70}^{-1}\, M_\odot}\right) = A\left(\frac{kT}{5\,\mathrm{keV}}\right)^\alpha . \qquad (3)$$

Using our sample of four dynamically relaxed lensing clusters given in Section 3.2.1, a best fit to the power-law M–T relation yields $A = 1.60 \pm 3.42$ and $\alpha = 1.43 \pm 1.28$, consistent with the theoretical expectation of $\alpha = 1.5$. Figure 1 shows this best-fit relation, for which the rms scatter is 360% for all eight clusters and 500% for the four unrelaxed clusters.

We compare with other observations and simulations of the M–T relation in Table 3, including those that used spectroscopic temperatures T_s and those that used mass-weighted temperatures T_m. For cases where the temperature normalization is not 5 keV and/or the mass scaling is not $10^{14}\, h_{70}^{-1}\, M_\odot$, we recalculate A using the published slope α, a temperature normalization of 5 keV, and a mass normalization of $10^{14}\, h_{70}^{-1}\, M_\odot$. To be conservative, we assume the fractional error in A is unchanged.

The observations we compare span varying temperature ranges, and there is some evidence that the M–T relation steepens for cooler clusters (e.g., Nevalainen et al. 2000; Finoguenov et al. 2001); for example, Arnaud et al. (2005) find a slope

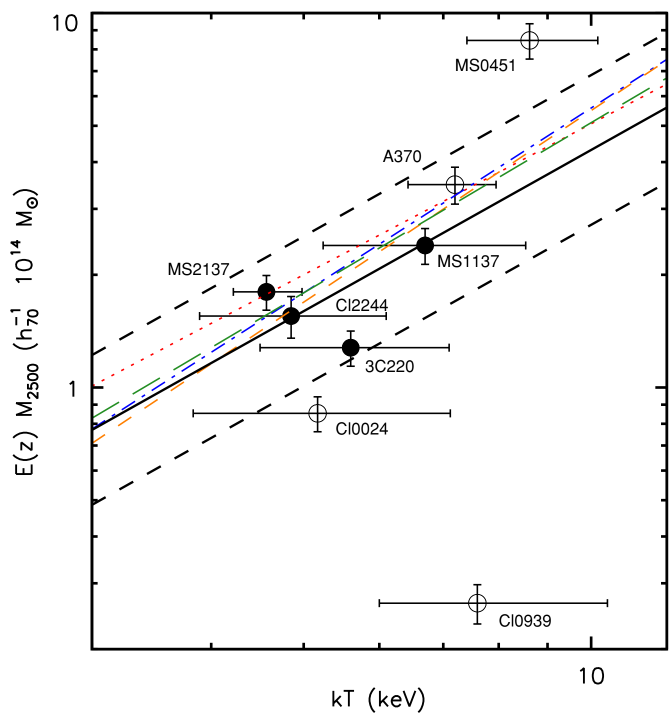

Figure 1. Mass–temperature relation for observed strong lensing clusters. Unrelaxed clusters (open circles) are not included in the fit, and the relaxed clusters (black points) are fit by a power law with slope $\alpha = 1.43$ (black solid line). The 1σ scatter for all eight clusters is large, $\Delta(\log[E(z)M_{2500}]) = 0.2$ (black dashed lines). Also shown are the other M–T relations for observational samples that use spectroscopic temperatures as we do: 17 weak lensing clusters with $3.6 < T_s$ (keV) < 9.8 (Hoekstra 2007; red dotted line), 13 relaxed X-ray clusters with $0.7 < T_s$ (keV) < 8.9 (Vikhlinin et al. 2006; blue dash-dotted line), 10 relaxed X-ray clusters with $2.2 < T_s$ (keV) < 8.3 (Arnaud et al. 2005; orange dashed line), and six relaxed X-ray clusters with $3.7 < T_s$ (keV) < 8.3 (Arnaud et al. 2005; green long dashed line). We find that our slope is in agreement with both the theoretical expectation of $\alpha = 1.5$ and measurements of α by other observations. For a detailed comparison to these and other estimates of the M–T relation, see Table 3.

(A color version of this figure is available in the online journal.)

of $\alpha = 1.51$ for clusters with 3.7 keV $< T_s <$ 8.3 keV, which increases to $\alpha = 1.70$ for clusters with 2.2 keV $< T_s <$ 8.3 keV. The temperature range we probe (4.6 keV $< T_s <$ 6.7 keV) is likely too small to exhibit a significant change in slope, but we lack a large enough statistical sample to test this properly.

We find that our best-fit slope α is consistent with both the theoretical expectation and the slopes derived by other observations and simulations of clusters. Our best-fit normalization A is somewhat lower than, but still consistent with, the normalizations found by the other observations and simulations. We find that relaxed strong lensing clusters follow the same M–T relation as relaxed clusters in general.

4.2. Correlation between the Temperature Scatter and Concentration Scatter

We have derived an M–T power-law relation for relaxed lensing clusters, but a more general M–T relation including both relaxed and unrelaxed clusters may be possible if we account for the differences in cluster concentrations. First, we define the virial radius of a cluster as the radius $r_{\rm vir}$ at which the average cluster density equals $\Delta_{\rm vir}(z)$ times the mean density at the cluster redshift z, where $\Delta_{\rm vir}(z) \simeq (18\pi^2 + 82x - 39x^2)/(1 + x)$ and $x \equiv \Omega_{\rm m}(z) - 1$ (Bryan & Norman 1998). Using the scale radius r_s of the best-fit NFW profile to each cluster, the cluster concentration is defined as $c_{\rm vir} \equiv r_{\rm vir}/r_s$.

Since more concentrated clusters are expected to form at higher redshifts (e.g., Navarro et al. 1997; Wechsler et al. 2002), if the cluster X-ray gas cools with time there might be a correlation between high cluster concentrations and low cluster temperatures. In addition, mergers with other clusters or groups may deplete the central mass densities in clusters while shock-heating the cluster gas, producing high cluster temperatures for low cluster concentrations. Here, we analyze whether there is any such correlation between the scatter in temperature and the scatter in concentration for our sample of eight strong lensing clusters.

Cluster concentrations, $c_{\rm vir}$, and cluster virial masses, $M_{\rm vir} \equiv M(\leqslant r_{\rm vir})$, are determined by strong lensing measurements for each of the clusters in our sample in Comerford & Natarajan (2007). The concentration, $c_{\rm vir} = 16$, determined by strong lensing measurements of MS 2137.3−2353 is known to be overestimated because the cluster's dark matter halo is likely elongated along or near the line of sight (Gavazzi 2005), so we instead use the concentration, $c_{\rm vir} = 8.75$, derived from the X-ray mass profile for MS 2137.3−2353 (Schmidt & Allen 2007). We note that if the lensing concentration were used for MS 2137.3−2353, Equation (5) would be $\Delta T = (-0.07\ {\rm keV})\Delta c - (0.49\ {\rm keV})$.

From a sample of 62 galaxy clusters, Comerford & Natarajan (2007) find a power-law relation between cluster concentration, $c_{\rm vir}$, and cluster virial mass, $M_{\rm vir}$, of

$$c_{\rm vir} = \frac{14.5 \pm 6.4}{(1+z)} \left(\frac{M_{\rm vir}}{1.3 \times 10^{13}\, h^{-1}\, M_\odot} \right)^{-0.15 \pm 0.13}, \qquad (4)$$

where z is the cluster redshift. For each of the eight clusters in our sample, we calculate the difference Δc between the measured concentration and the concentration predicted by the above c–M relation. We also calculate the difference ΔT between the measured X-ray temperature and the temperature predicted by the M–T relation we determined in Section 4.1 for the four relaxed clusters.

Figure 2 shows the results of these ΔT and Δc calculations. The best-fit line to the data is

$$\Delta T = (-2.75\ {\rm keV} \pm 0.07\ {\rm keV})\Delta c - (1.56\ {\rm keV} \pm 0.49\ {\rm keV}), \qquad (5)$$

suggesting that indeed higher (lower) temperature clusters tend to have lower (higher) concentrations.

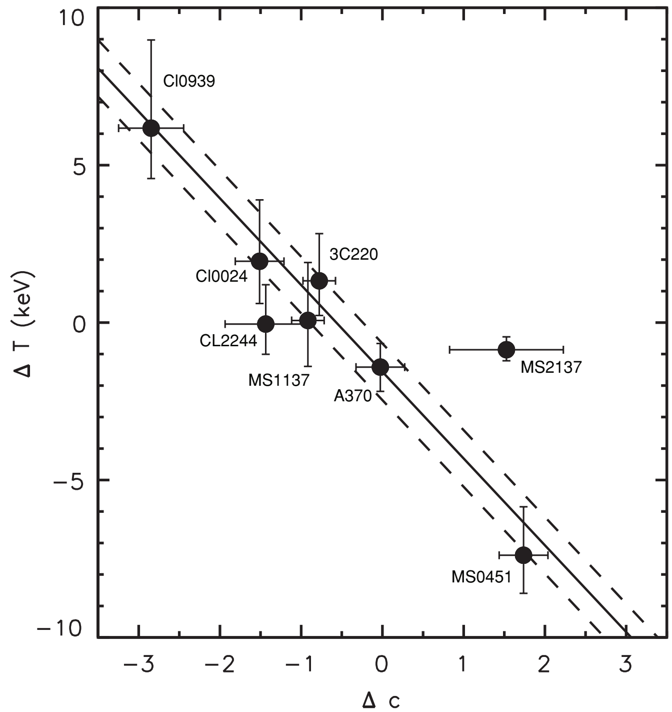

Figure 2. Correlation between the difference ΔT between the observed X-ray temperatures and the predicted temperatures from the M–T relation and the difference Δc between the measured concentrations and the predicted concentrations from the c–M relation. The eight strong lensing clusters in our sample are represented, and the solid line shows the best-fit line to the data $\Delta T = (-2.75\ {\rm keV})\Delta c - (1.56\ {\rm keV})$. The dashed lines show the 1σ scatter $\Delta(\Delta T) = 0.9$ keV.

4.3. The M–T Relation for All Strong Lensing Clusters

Using the relation between the scatter in cluster temperature and the scatter in cluster concentration for the eight strong lensing clusters (Section 4.2), we adjust for the apparent dependence of cluster temperatures on cluster concentrations. We use Δc for each cluster to calculate its corresponding ΔT from the best-fit relation given in Equation (5). We then subtract this ΔT from the measured temperature to obtain a corrected temperature $T_{\rm corr}$, and we illustrate the resultant temperature-corrected M–T relation in Figure 3. The figure also shows the relation we derived in Section 4.1 for the four relaxed clusters, where $A = 1.60$ and $\alpha = 1.43$.

We find that cluster concentration, mass, and X-ray temperature are tightly correlated, and as a result incorporating the ΔT–Δc relation significantly reduces the scatter in the M–T relation. Comparing Figure 3 to Figure 1 underscores the impact of our temperature correction in reducing the scatter in the M–T relation. The temperature correction reduces the rms scatter for all eight clusters by a factor of 6, from 360% to 60%, and more significantly, reduces the rms scatter for the four unrelaxed clusters by a factor of 30, from 500% to 15%. (The rms scatter for the four relaxed clusters increases from 26% to 83%, possibly because the temperatures we use do not correct for cool cores at the cluster centers.) With the temperature correction, even unrelaxed clusters follow the M–T relation we originally derived using only the relaxed clusters (Section 4.1). Therefore, we suggest this temperature correction as a tool for establishing a universal M–T relation that applies to all galaxy clusters regardless of their dynamical state.

The error in the measurement of σ_8 from cluster counts depends directly on the error in the cluster M–T relation; for

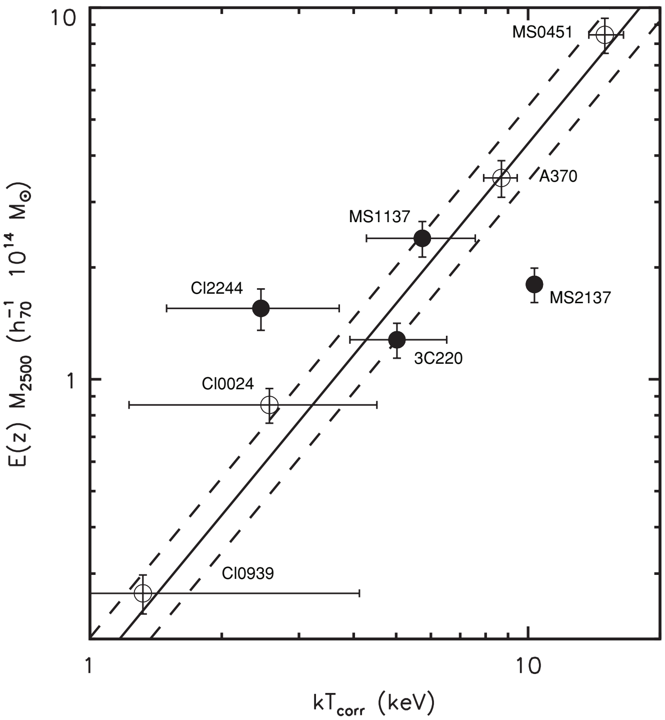

Figure 3. Mass–temperature relation, after correcting for the scatter in temperature, for observed strong lensing clusters. As in Figure 1, open circles represent unrelaxed clusters and black points represent relaxed clusters. We adjust the temperature of each cluster according to its concentration and the ΔT–Δc relation. The best-fit M–T relation for relaxed clusters, derived in Section 4.1, is shown as the solid line. The 1σ scatter for all eight clusters is $\Delta(\log[E(z)M_{2500}]) = 0.1$ (black dashed lines), significantly smaller than the scatter in the uncorrected M–T relation (see Figure 1).

example, a 25% 1σ uncertainty in the zero point of the M–T relation corresponds to a 10% 1σ uncertainty in σ_8 (Evrard et al. 2002). Consequently, we find that the temperature correction not only reduces the scatter in the M–T relation, but also significantly reduces the error in the corresponding measurement of σ_8.

An alternate cluster scaling relation that also has lower scatter than the traditional M–T relation is the Y_X–M_{500} relation (Kravtsov et al. 2006). Here, M_{500} is the cluster mass within the radius r_{500} enclosing an overdensity of 500 relative to the critical density, $Y_X = M_g T_X$, M_g is the cluster gas mass within r_{500}, and T_X is the mean spectral X-ray temperature of the cluster. Our scaling relation offers the advantage that it is based on lensing mass estimates, which are free of assumptions about a cluster's dynamical state.

5. BCG PROPERTIES

In addition to the interdependences of many cluster properties, properties of the BCG have also been shown to correlate with the host cluster. Here we identify the BCG in each of our clusters, measure the luminosity of each BCG, and examine the correlation between BCG luminosity and host cluster mass for our strong lensing sample.

5.1. BCG Determination

We select each cluster's BCG as the brightest member galaxy. Each BCG corresponds to the lens galaxy or one of the lens galaxies used to determine the cluster mass distribution in Comerford et al. (2006). When multiple lens galaxies were used to model a single cluster, we identify which of the lens galaxies is the BCG in Table 4, and we also note references that confirm the BCG selection.

Table 4
BCG Luminosities

Cluster	BCG[a]	$L_{K,\mathrm{BCG}}$ ($10^{11}\ h_{70}^{-2}\ L_{\odot}$)	$L_{K,\mathrm{passive,BCG}}$ ($10^{11}\ h_{70}^{-2}\ L_{\odot}$)	Reference
ClG 2244−02		1.03 ± 0.09	0.96 ± 0.09	1
Abell 370	G1	1.5 ± 0.1	1.3 ± 0.1	
3C 220.1		6.4 ± 0.4	5.3 ± 0.3	
MS 2137.3−2353		8.98 ± 0.09	0.84 ± 0.08	
MS 0451.6−0305		4.3 ± 0.3	3.7 ± 0.3	2
MS 1137.5+6625		15 ± 2	11 ± 1	
Cl 0939+4713	G1	1.9 ± 0.2	1.7 ± 0.2	3
ZwCl 0024+1652	362	1.69 ± 0.07	1.51 ± 0.06	4, 5

Note.
[a] See Comerford et al. (2006) for identification of the galaxies by name.
References. (1) Bautz et al. 1982; (2) Ellingson et al. 1998; (3) De Filippis et al. 2003; (4) Kneib et al. 2003; (5) Moran et al. 2005.

5.2. BCG Luminosity Determination

For each cluster we have *HST* imaging taken in some combination of the filters F450W, F555W, F675W, F702W, and F814W. Using Source EXtractor (Bertin & Arnouts 1996), we measure MAG_AUTO magnitudes for the BCG galaxies. We estimate the magnitude uncertainties by adding in quadrature the error in the measured flux and the estimated background subtraction error, which is the product of the area of the extraction aperture and the rms variation of the subtracted background flux. We calculate the BCG luminosities using the available photometry in an observed band as the normalization factor on two types of spectral energy distribution templates, and then compute the rest-frame magnitudes and luminosities in several bands including K band. The templates we use are calculated from the Bruzual & Charlot (2003) stellar population synthesis models with a Salpeter initial mass function. The first we use is a fixed-age 10 Gyr old simple stellar population, and the second is for a simple stellar population with an age given by an assumed formation redshift of $z = 3.0$. The latter enables an estimate of the passively evolved BCG luminosity.

6. THE BCG LUMINOSITY–CLUSTER MASS RELATION

Although it is still unclear how BCGs form, conventional formation scenarios include galactic cannibalism, cooling flows, and mergers during cluster formation (Section 1). The evolution of the luminosity of the BCG with the mass of the cluster may distinguish between these models and offer insight into the formation of BCGs. Semianalytic and numerical simulations of structure formation suggest a tight correlation between BCG luminosities and cluster masses (e.g., Somerville & Primack 1999; Cole et al. 2000), and we can parameterize such a correlation between K-band BCG luminosities and cluster masses M_{200} by the power law

$$\frac{L_{K,\mathrm{BCG}}}{10^{11}\ h_{70}^{-2}\ L_{\odot}} = B\left(\frac{M_{200}}{10^{14}\ h_{70}^{-1}\ M_{\odot}}\right)^{\beta}. \quad (6)$$

Here, we examine the relation between BCG luminosity and cluster mass for clues about the formation histories of BCGs

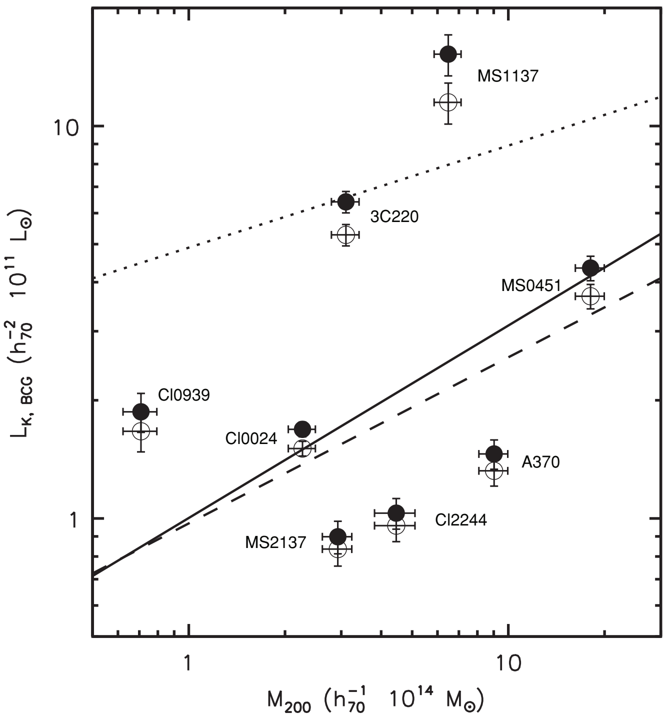

Figure 4. Correlation between K-band BCG luminosity and cluster mass for our sample of strong lensing clusters. Uncorrected luminosities (black points) are fit by the solid line, while luminosities corrected for passive evolution (open circles) are fit by the dashed line. For comparison, the Lin & Mohr (2004) *L–M* relation for the general cluster population is shown as the dotted line. Our best-fit power laws are significantly steeper than that of Lin & Mohr (2004), hinting that BCGs in lensing clusters may have different formation histories than BCGs in typical clusters.

in strong lensing clusters and how their formations may differ from the general BCG population. We represent the general BCG population with the Lin & Mohr (2004) study of 93 BCGs at $z \leqslant 0.09$ in the Two Micron All Sky Survey (2MASS).

For an accurate comparison to the *L–M* relation Lin & Mohr (2004) find from 2MASS, we follow their definition of BCG luminosity. Lin & Mohr (2004) measure BCG luminosities in the K band using 20 mag arcsec^{-2} isophotal elliptical aperture magnitudes for 2MASS, called K20 magnitudes. Similarly, we convert to the K band (see Section 5.2) and measure BCG magnitudes using SExtractor's MAG_AUTO function (Bertin & Arnouts 1996), which has good agreement with 2MASS K20 total magnitudes for sources such as BCGs that are bright and extended (Elston et al. 2006). We then convert the magnitudes into K-band luminosities as described in Section 5.2. The resultant K-band BCG luminosities, along with the luminosities corrected for passive evolution, are given in Table 4.

Figure 4 illustrates the correlation between BCG luminosities and cluster masses M_{200}. We find the best-fit power law to the data is given by $B = 0.97 \pm 0.17$ and $\beta = 0.48 \pm 0.09$ for all strong lensing clusters (solid line in Figure 4) and $B = 0.93 \pm 0.18$ and $\beta = 0.39 \pm 0.10$ for all strong lensing clusters when the BCG luminosities are corrected for passive evolution (dashed line in Figure 4). The similarity of these two results implies that the passive evolution of BCG luminosities with redshift has little effect on the *L–M* relation, and more generally there is no evidence for evolution in the *L–M* relation from $z \sim 1$ to $z \sim 0$ (Brough et al. 2008).

For comparison, Lin & Mohr (2004) find a best-fit power law of $B = 4.9 \pm 0.2$ and $\beta = 0.26 \pm 0.04$ (dotted line in Figure 4), which is consistent with the slopes found by analytic estimates and cosmological simulations of the growth of central galaxies. Using the galaxy–dark matter correlation function to determine host dark matter halo masses for observational catalogs of galaxies, Cooray & Milosavljević (2005) find $L \propto M_{200}^{<0.3}$ for halo masses $\gtrsim 4 \times 10^{13}$ $h^{-1}\,M_\odot$. Similarly, Vale & Ostriker (2006) determine a correlation of $L \propto M_{100}^{0.28}$ when they combine the subhalo mass distribution derived from simulations with an empirical galaxy luminosity function. They also find little dependence of the *L–M* relation on waveband.

From their slope of $\beta = 0.26$, Lin & Mohr (2004) conclude that while other cluster members may merge with BCGs and increase BCG luminosities, such effects are not sufficient to fully account for the growth in $L_{\mathrm{K,BCG}}$ with cluster mass. Instead, Lin & Mohr (2004) suggest that BCGs must grow mainly through mergers with other BCGs brought in when the host galaxy cluster merges with other groups or clusters. In addition to the many hierarchical structure formation simulations and models that support this scenario (e.g., Merritt 1985; Dubinski 1998; Boylan-Kolchin et al. 2006), there are also observations of a pair of $\sim L^*$ elliptical galaxies merging to build up the BCG in a rich cluster at $z = 1.26$ (Yamada et al. 2002).

Our slope β is 50% (when luminosities are corrected for passive evolution) to 85% (when luminosities are not corrected for passive evolution) steeper than that of Lin & Mohr (2004), hinting that strong lensing clusters may undergo more mergers with groups and clusters, or merge with more massive groups and clusters, than the average cluster. Both more mergers and mergers with more massive systems could account for the initial evidence for an increase in $L_{\mathrm{K,BCG}}$ with cluster mass we find in strong lensing clusters, and would also be consistent with simulations that suggest strong lensing clusters are dynamically more active than the general cluster population (Bartelmann & Steinmetz 1996). However, the scatter in our *L–M* relation is significant, and a larger sample of strong lensing clusters is necessary to draw definitive conclusions about the formation histories of strong lensing clusters.

7. CONCLUSIONS

We have determined the scaling of cluster mass with cluster temperature and the scaling of BCG luminosity with cluster mass for eight observed strong lensing galaxy clusters imaged with *HST* and at redshifts $0.3 < z < 0.8$. We explored cluster concentrations as a means of reducing the scatter in the *M–T* relation and enabling more precise constraints on cosmological parameters, and we used the *L–M* relation as an indicator of the formation histories of strong lensing BCGs and clusters. Our main results are as follows.

1. The best-fit cluster mass–temperature relation for our four dynamically relaxed strong lensing clusters is

$$E(z)\left(\frac{M_{2500}}{10^{14}\,h_{70}^{-1}\,M_\odot}\right) = 1.60 \pm 3.42\left(\frac{kT}{5\,\mathrm{keV}}\right)^{1.43\pm1.28}, \quad (7)$$

which is consistent with the theoretical expectation of the *M–T* relation for relaxed clusters, as well as the *M–T* relations determined by other observations and simulations. We find that relaxed strong lensing clusters do not deviate from the *M–T* relation for the general population of relaxed clusters.

Significantly, we find an inverse correlation between cluster temperature and cluster concentration that, when incorporated into the M–T relation, reduces the M–T scatter by a factor of 6, from 360% to 60%. By correcting cluster temperatures according to the temperature–concentration relation, we find that the M–T relation given in Equation (7) describes not only the relaxed strong lensing clusters, but the entire cluster population regardless of dynamical state. Specifically, the scatter in unrelaxed clusters decreases by a factor of 30, from 500% in the uncorrected M–T relation to 15% in the temperature-corrected M–T relation. Incorporating concentration effects into the M–T relation tightens the M–T relation for all clusters, which in turn reduces the error in the determination of σ_8 from cluster counts. Whereas accurate cluster determinations of σ_8 were previously made only with relaxed clusters, concentrations enable the inclusion of unrelaxed clusters. The larger cluster samples possible with the inclusion of unrelaxed clusters offer yet more precise σ_8 estimates from cluster observations.

2. The best-fit relation between BCG luminosity and cluster mass for our sample of strong lensing clusters is

$$\frac{L_{\mathrm{K,BCG}}}{10^{11}\ h_{70}^{-2}\ L_\odot} = 0.97 \pm 0.17 \left(\frac{M_{200}}{10^{14}\ h_{70}^{-1}\ M_\odot}\right)^{0.48\pm0.09}, \tag{8}$$

which is ~85% steeper than the correlations predicted for non-strong-lensing clusters by other observations, theory, and cosmological simulations. This result supports the current evidence that BCGs are built up through mergers with massive galaxies in other groups and clusters, and also hints that strong lensing clusters may have more active merging histories than typical clusters. A larger sample of strong lensing clusters might enable more definite conclusions about the formation histories of strong lensing clusters.

Accurate cluster mass measurements and full use of the range of cluster property interdependences are key components in the calibration of clusters as tracers of cosmological parameters. As we have shown, gravitational lensing enables the most direct measurements of cluster mass, without assumptions about the cluster's dynamical state that are inherent in other methods. We have also shown that the correlation between cluster temperature and concentration can significantly reduce the scatter in the cluster M–T relation, enabling more precise estimates of σ_8. It may be that other cluster scalings can be effectively combined to reduce the error on additional cosmological parameter estimates.

J.M.C. acknowledges support of this work by a National Science Foundation Graduate Research Fellowship. The work of L.A.M. was carried out at the Jet Propulsion Laboratory, California Institute of Technology, with the support of NASA ATFP08-0169. P.N. thanks the Radcliffe Institute for Advanced Study and the Center for Astrophysics (CfA) for providing an intellectually stimulating atmosphere that enabled this work.

REFERENCES

Allen, S. 1998, MNRAS, 296, 392
Allen, S. W., Schmidt, R. W., Ebeling, H., Fabian, A. C., & van Speybroeck, L. 2004, MNRAS, 353, 457
Allen, S. W., Schmidt, R. W., & Fabian, A. C. 2001, MNRAS, 328, L37
Andersson, K., Peterson, J. R., Madejski, G., & Goobar, A. 2009, ApJ, 696, 1029
Arnaud, M., Pointecouteau, E., & Pratt, G. W. 2005, A&A, 441, 893
Bahcall, N. A., & Comerford, J. M. 2002, ApJ, 565, L5
Bailey, M. E. 1982, MNRAS, 201, 271
Bartelmann, M., & Steinmetz, M. 1996, MNRAS, 283, 431
Bautz, M., Loh, E., & Wilkinson, D. T. 1982, ApJ, 255, 57
Bertin, E., & Arnouts, S. 1996, A&AS, 117, 393
Bildfell, C., Hoekstra, H., Babul, A., & Mahdavi, A. 2008, MNRAS, 389, 1637
Borys, C., et al. 2004, MNRAS, 352, 759
Boylan-Kolchin, M., Ma, C.-P., & Quataert, E. 2006, MNRAS, 369, 1081
Broadhurst, T., Huang, X., Frye, B., & Ellis, R. S. 2000, ApJ, 534, L15
Brough, S., Couch, W. J., Collins, C. A., Jarrett, T., Burke, D. J., & Mann, R. G. 2008, MNRAS, 385, L103
Bruzual, G., & Charlot, S. 2003, MNRAS, 344, 1000
Bryan, G. L., & Norman, M. L. 1998, ApJ, 495, 80
Cardiel, N., Gorgas, J., & Aragon-Salamanca, A. 1998, MNRAS, 298, 977
Churazov, E., Brüggen, M., Kaiser, C. R., Böhringer, H., & Forman, W. 2001, ApJ, 554, 261
Cole, S., Lacey, C. G., Baugh, C. M., & Frenk, C. S. 2000, MNRAS, 319, 168
Comerford, J. M., Meneghetti, M., Bartelmann, M., & Schirmer, M. 2006, ApJ, 642, 39
Comerford, J. M., & Natarajan, P. 2007, MNRAS, 379, 190
Cooray, A., & Milosavljević, M. 2005, ApJ, 627, L85
Cotter, G., Buttery, H. J., Das, R., Jones, M. E., Grainge, K., Pooley, G. G., & Saunders, R. 2002, MNRAS, 334, 323
Cowie, L. L., & Binney, J. 1977, ApJ, 215, 723
Crawford, C. S., Allen, S. W., Ebeling, H., Edge, A. C., & Fabian, A. C. 1999, MNRAS, 306, 857
Czoske, O., Moore, B., Kneib, J.-P., & Soucail, G. 2002, A&A, 386, 31
De Filippis, E., Schindler, S., & Castillo-Morales, A. 2003, A&A, 404, 63
Donahue, M., Voit, G. M., Scharf, C. A., Gioia, I. M., Mullis, C. R., Hughes, J. P., & Stocke, J. T. 1999, ApJ, 527, 525
Dubinski, J. 1998, ApJ, 502, 141
Ellingson, E., Yee, H. K. C., Abraham, R. G., Morris, S. L., & Carlberg, R. G. 1998, ApJS, 116, 247
Elston, R. J., et al. 2006, ApJ, 639, 816
Evrard, A. E., Metzler, C. A., & Navarro, J. F. 1996, ApJ, 469, 494
Evrard, A. E., et al. 2002, ApJ, 573, 7
Finoguenov, A., Reiprich, T. H., & Böhringer, H. 2001, A&A, 368, 749
Gavazzi, R. 2005, in IAU Symp. 225, Gravitational Lensing Impact on Cosmology, ed. Y. Mellier & G. Meylan (Cambridge: Cambridge Univ. Press), 179
Haiman, Z., Mohr, J. J., & Holder, G. P. 2001, ApJ, 553, 545
Hausman, M. A., & Ostriker, J. P. 1978, ApJ, 224, 320
Henry, J. P. 2004, ApJ, 609, 603
Hicks, A. K., & Mushotzky, R. 2005, ApJ, 635, L9
Hoekstra, H. 2007, MNRAS, 379, 317
Horner, D. J. 2001, PhD thesis, Univ. of Maryland College Park
Jeltema, T. E., Hallman, E. J., Burns, J. O., & Motl, P. M. 2008, ApJ, 681, 167
Kay, S. T., da Silva, A. C., Aghanim, N., Blanchard, A., Liddle, A. R., Puget, J.-L., Sadat, R., & Thomas, P. A. 2005, Adv. Space Res., 36, 694
Kneib, J., Mellier, Y., Fort, B., & Mathez, G. 1993, A&A, 273, 367
Kneib, J., et al. 2003, ApJ, 598, 804
Kravtsov, A. V., Vikhlinin, A., & Nagai, D. 2006, ApJ, 650, 128
Levine, E. S., Schulz, A. E., & White, M. 2002, ApJ, 577, 569
Lin, Y.-T., & Mohr, J. J. 2004, ApJ, 617, 879
Mahdavi, A., Hoekstra, H., Babul, A., & Henry, J. P. 2008, MNRAS, 384, 1567
Mathiesen, B. F., & Evrard, A. E. 2001, ApJ, 546, 100
Maughan, B. J., Jones, C., Forman, W., & Van Speybroeck, L. 2008, ApJS, 174, 117
Mazzotta, P., Rasia, E., Moscardini, L., & Tormen, G. 2004, MNRAS, 354, 10
McNamara, B. R., et al. 2006, ApJ, 648, 164
Mellier, Y., Fort, B., Bonnet, H., & Kneib, J.-P. 1994, in NATO ASI Ser. 441, Cosmological Aspects of X-ray Clusters of Galaxies, ed. W. C. Seitter (Dordrecht: Kluwer), 219
Merritt, D. 1985, ApJ, 289, 18
Mohr, J. J., Fabricant, D. G., & Geller, M. J. 1993, ApJ, 413, 492
Moran, S. M., Ellis, R. S., Treu, T., Smail, I., Dressler, A., Coil, A. L., & Smith, G. P. 2005, ApJ, 634, 977
Natarajan, P., Kneib, J.-P., Smail, I., Treu, T., Ellis, R., Moran, S., Limousin, M., & Czoske, O. 2009, ApJ, 693, 970
Navarro, J., Frenk, C., & White, S. 1996, ApJ, 462, 563
Navarro, J., Frenk, C., & White, S. 1997, ApJ, 490, 493
Nevalainen, J., Markevitch, M., & Forman, W. 2000, ApJ, 532, 694
Ostriker, J. P., & Tremaine, S. D. 1975, ApJ, 202, L113
Ota, N., & Mitsuda, K. 2004, A&A, 428, 757
Ota, N., Mitsuda, K., & Fukazawa, Y. 1998, ApJ, 495, 170
Ota, N., Mitsuda, K., Hattori, M., & Mihara, T. 2000, ApJ, 530, 172

Ota, N., Pointecouteau, E., Hattori, M., & Mitsuda, K. 2004, ApJ, 601, 120
Pierpaoli, E., Borgani, S., Scott, D., & White, M. 2003, MNRAS, 342, 163
Schindler, S., Belloni, P., Ikebe, Y., Hattori, M., Wambsganss, J., & Tanaka, Y. 1998, A&A, 338, 843
Schindler, S., & Wambsganss, J. 1996, A&A, 313, 113
Schmidt, R. W., & Allen, S. W. 2007, MNRAS, 379, 209
Schuecker, P., Böhringer, H., Collins, C. A., & Guzzo, L. 2003, A&A, 398, 867
Smith, G. P., Kneib, J., Smail, I., Mazzotta, P., Ebeling, H., & Czoske, O. 2005, MNRAS, 359, 417
Somerville, R. S., & Primack, J. R. 1999, MNRAS, 310, 1087
Vale, A., & Ostriker, J. P. 2006, MNRAS, 371, 1173
Vikhlinin, A., Kravtsov, A., Forman, W., Jones, C., Markevitch, M., Murray, S. S., & Van Speybroeck, L. 2006, ApJ, 640, 691
Vikhlinin, A., et al. 2009, ApJ, 692, 1060
Voit, G. M. 2005, Rev. Mod. Phys., 77, 207
Wechsler, R., Bullock, J., Primack, J., Kravtsov, A., & Dekel, A. 2002, ApJ, 568, 52
Worrall, D. M., Birkinshaw, M., Hardcastle, M. J., & Lawrence, C. R. 2001, MNRAS, 326, 1127
Wu, X.-P. 2000, MNRAS, 316, 299
Yamada, T., Koyama, Y., Nakata, F., Kajisawa, M., Tanaka, I., Kodama, T., Okamura, S., & De Propris, R. 2002, ApJ, 577, L89
Zhang, Y., Böhringer, H., Mellier, Y., Soucail, G., & Forman, W. 2005, A&A, 429, 85
Zhang, Y., Finoguenov, A., Böhringer, H., Kneib, J., Smith, G. P., Kneissl, R., Okabe, N., & Dahle, H. 2008, A&A, 482, 451
Zhang, Y., Reiprich, T. H., Finoguenov, A., Hudson, D. S., & Sarazin, C. L. 2009, ApJ, 699, 1178